Polarization-selective dual-wavelength gap-surface plasmon metasurfaces

Tang, Shiwei; Ding, Fei; Jiang, Tao; Cai, Tong; Xu, Hexiu

Published in:
Optics Express

Publication date:
2018

Citation for pulished version (APA):
Tang, S., Ding, F., Jiang, T., Cai, T., & Xu, H. (2018). Polarization-selective dual-wavelength gap-surface plasmon metasurfaces. Optics Express, 26(18).

Research Article | Vol. 26, No. 18 | 3 Sep 2018 | OPTICS EXPRESS 23760
Optics EXPRESS

Polarization-selective dual-wavelength gap-surface plasmon metasurfaces

SHIWEI TANG,[1,4] FEI DING,[2,5] TAO JIANG,[1] TONG CAI,[3] AND HE-XIU XU[3]

[1]*Department of Physics, Faculty of Science, Ningbo University, Ningbo 315211, China*
[2]*SDU Nano Optics, University of Southern Denmark, Campusvej 55, Odense DK-5230, Denmark*
[3]*Air and Missile Defend College, Air Force Engineering University, Xi'an 710051, China*
[4]*tangshiwei@nbu.edu.cn*
[*]*feid@mci.sdu.dk*

Abstract: In this paper, we present a general method to realize polarization-selective dual-wavelength gap-surface plasmon metasurfaces (GSPMs), which are composed of strongly anisotropic meta-atoms periodically arranged in a rectangular lattice with two degrees of freedom to independently control the reflection phase and amplitude of orthogonal linear polarizations at two discrete wavelengths. We design and demonstrate dual-wavelength GSPMs as polarization beam splitters and focusing metamirrors operating at 850 and 1550 nm simultaneously. Our work provides a general approach to design multiwavelength, multifunctional metasurfaces with various potential applications.

OCIS codes: (160.3918) Metamaterials; (130.5440) Polarization-selective devices; (160.1245) Artificially engineered materials.

1. Introduction

In modern science and technology, the photonics integration plays a critical role in solving the increasing demands regarding the data-storage capacity and information processing speed. However, the conventional methods to manipulate light rely on the gradually accumulated phase change during light propagation, thereby resulting in bulky optical components with complex shapes. The resulting bulky optical devices go against the recent trends in photonics, which aims at very dense integration and miniaturization. In recent years, metasurfaces, that is, planar artificial nanostructures that can produce a desired optical response and realize a specific optical wavefront transformation by controlling multiple properties such as polarization, phase, and amplitude of the reflected and transmitted fields, have attracted increasing attention due to their planar profiles and ease of fabrication [1–5]. As such, numerous fancy physics phenomena and promising applications have been demonstrated by different metasurfaces, such as anomalous beam-steering [6–13], surface waves couplers [14–17], optical holograms [18–21], focusing lenses [22–25], wave-plates [26–28], and polarimeters [29–32]. In addition to the lightweight, compactness and arbitrary control over wavefront, another major advantage of metasurfaces is their multifunctionality. Recently, it has been shown that a single metasurface can effectively integrate multiple diversified functionalities into an ultrathin device with compact footprint [33–43]. For instance, metasurfaces can realize distinct functionalities depending on the input polarization states [38–43].

Although metasurfaces are promising to implement fascinating functionalities, most of the up-to-date metasurfaces are typically designed to work at a single wavelength. Thus, it is highly desired to achieve multiwavelength metasurfaces capable of providing independent wavefront modulation at multiple desired wavelengths. Up to now, many efforts have been devoted to circumventing this limitation at two or three distinct wavelengths [44–53]. To realize multiwavelength metasurface, a simple scheme developed is to merge specific meta-atoms spatially, where each meta-atom exhibits response at a certain wavelength [44–48]. Meanwhile, complicated meta-atoms have been designed to achieve multiple optical responses at different wavelengths, with the complete phase and amplitude modulations [49–

#339873 https://doi.org/10.1364/OE.26.023760
Journal © 2018 Received 17 Jul 2018; revised 18 Aug 2018; accepted 20 Aug 2018; published 29 Aug 2018

Optics EXPRESS

51]. However, the implemented approaches suffer from crosstalk between different meta-atoms and the working efficiency at each wavelength is inevitably limited. In order to reduce the cross-talk and increase the efficiencies between different wavelengths, strongly anisotropic meta-atoms, exhibiting polarization-controlled optical responses, have been used as the basic building blocks to design multifunctional metasurfaces, particularly dual-wavelength metasurfaces [52,53].

In this paper, we design polarization-selective dual-wavelength gap-surface plasmon metasurfaces (GSPMs), which consist of periodic anisotropic meta-atoms arranged in a rectangular lattice with two degrees of freedom to independently control the reflection coefficients of orthogonal linear polarizations at two discrete wavelengths. Based on the designed anisotropic meta-atoms, we demonstrate dual-wavelength GSPMs as polarization beam splitters and focusing metamirror operating at 850 and 1550 nm simultaneously. Our work provides a general approach to design multi-wavelength, multifunctional metasurfaces with potential applications.

2. Meta-atom design

Figure 1(a) schematically illustrates the proposed dual-wavelength GSPM functioning as a polarization and wavelength beam splitter, which consists of periodically arranged metal-insulator-metal (MIM) meta-atoms. The basic meta-atom is composed of 50-nm-thin silver (Ag) nanobricks arranged periodically in the *x*-*y* plane and a 130-nm-thin continuous Ag film, separated by a silicon dioxide (SiO_2) spacer with deep-subwavelength thickness [Fig. 1(b)]. When the meta-atom is illuminated by a normal incident plane wave that is either *x*- or *y*-polarized, electric currents are induced on both the topmost nanobricks and the bottom Ag film, resulting in strong near-field coupling and anti-parallel electric current oscillations, forming the strong magnetic resonance [54–60]. By varying the geometry of the meta-atom, the reflection phase and amplitude of each unit cell can be engineered independently at the designed wavelength [58,59]. To realize the polarization-selective response at two discrete wavelengths, the unit cell is set to be rectangular with different periodicities along the *x*- and *y*-directions (e.g., p_x = 250 nm and p_y = 500 nm). Since the reflected coefficients vary with the spacer thickness, the SiO_2 dielectric layer is optimized to have a thickness of t_s = 50 nm, which ensures almost 2π phase modulation while maintaining high reflectance at the two investigated wavelengths, that is, λ = 850 and 1550 nm.

We implemented three dimensional (3D) full-wave simulations by using the commercially available software Comsol Multiphysics (ver. 5.3) based on finite element method (FEM) to determine the complex reflection coefficients. For the homogeneous meta-atom in Fig. 1(b), we modeled one unit cell by applying periodic boundary conditions on the vertical sides of the cell. The complex reflection coefficients were determined on the top surfaces of the nanobricks when linearly polarized light is normally impinging onto the surface. In our Ag-SiO_2-Ag configurations, the permittivity of Ag is described by Drude model $\varepsilon_r(\omega) = \varepsilon_\infty - \omega_P^2 / \omega(\omega - i\omega_{col})$ with epsilon infinity ε_∞=3.4 , the plasma frequency ω_p=1.37×10$^{16}s^{-1}$ and the damping frequency ω_{col}=9×10$^{13}s^{-1}$, where ω is the angular frequency and the surface roughness and grain boundary effects have been taken into consideration [57]. The SiO_2 spacer layer is taken as a lossless dielectric with a constant refractive index *n* = 1.45. The medium above the configurations was chosen to be air and truncated using perfectly matched layer (PML) to minimize reflections. Figure 1(c) displays the minimum reflectivity and reflection phase of the homogenous metasurface at the designed wavelengths of λ = 850 and 1550 nm as a function of the nanobrick dimensions l_x and l_y, confirming that we can independently control the amplitude and phase of the reflected light for the two orthogonal polarizations at two wavelengths. For *x*-polarization at λ = 850 nm, the reflection phase and amplitude are dominantly controlled by l_x while l_y has little effect. If the

Optics EXPRESS

incident light is switched to y-polarization, the reflection coefficients at λ = 1550 nm are strongly depending on l_y.

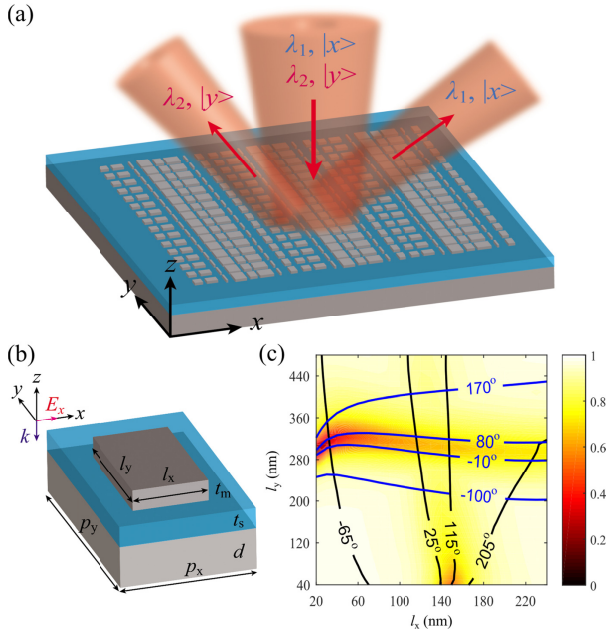

Fig. 1. (a) Schematic of the polarization-sensitive dual-wavelength GSPM. (b) Schematic of the unit cell consisting of an Ag nanobrick on top of a spacer and Ag substrate. The fixed geometrical parameters are p_x = 250 nm, p_y = 500 nm, d = 130 nm, t_s = 50 nm, and t_m = 50 nm. (c) Calculated reflectivity and phase as a function of the nanobrick dimensions for λ = 850 nm under x-polarization and λ = 1550 nm under y-polarization. The reflectivity map represents the minimum reflectivity for both λ = 850 nm under x-polarization and λ = 1550 nm under y-polarization, while lines are contours of the reflection phase for λ = 850 nm under x-polarization (black curves) and λ = 1550 nm under y-polarization (blue curves).

3. Polarization and wavelength beam splitters

In order to demonstrate the capability of the polarization-selective dual-wavelength GSPM, we first design three different gradient metasurfaces that, in all cases, function as polarization and wavelength beam splitters, indicating the ability of engineering the light direction of two wavelengths at will. Importantly, these gradient metasurfaces operate independently and differently for different polarizations at two discrete wavelengths, which is not accessible with conventional optical components. Firstly, we investigate a polarization beam splitter (design 1) that reflects incident x-polarized and y-polarized waves into + 1 and 0 diffraction orders, respectively. In this design, the gradient metasurface has a positive phase gradient along the x-direction for x-polarization at λ = 850 nm while there is no phase gradient for y-polarization at λ = 1550 nm. Specifically, this gradient metasurface consists of four meta-atoms, whose reflection phases for x-polarization at λ = 850 nm are discretized into four constant phase contour lines with a step of 90°. In contrast, the four meta-atoms have similar reflection phases, resulting in the specular reflection for y-polarization at λ = 1550 nm. Figure 2(a) illustrates the gradient metasurface, which is constructed by placing the four meta-atoms with the center-to-center distance of p_x = 250 nm into a supercell. Thus, the supercell has a periodicity of 1000 nm, resulting thereby in an anomalous reflection peak at an angle of 58.2° for x-polarized light at λ = 850 nm in the x-z plane. To verify the polarization beam steering, 3D full-wave numerical simulations were performed by modeling the periodic supercell shown in Fig. 2(a). The reflected electric fields E_{xr} at λ = 850 nm is plotted in Fig. 2(b), showing well-defined wave-front. As expected, ~95% of the reflected light is contained

Optics EXPRESS

within the + 1 diffraction order at the designed wavelength of λ = 850 nm under *x*-polarized excitation, while the other diffraction orders are strongly suppressed [Fig. 2(c)]. Additionally, the absolute reflectivity is limited to ~85% due to the Ohmic loss in the metal. In contrast to the case of *x*-polarization, all the light is specularly reflected to the 0 order at λ = 1550 nm for *x*-polarization with the reflectivity reaching as high as ~94% [Figs. 2(d) and 2(e)].

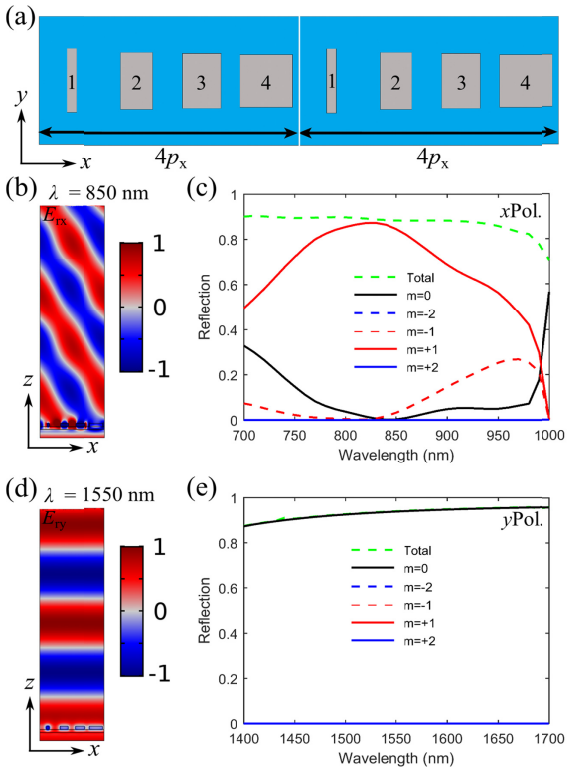

Fig. 2. (a) Supercell of the polarization-sensitive dual-wavelength GSPM functioning as a polarization beam splitter (design 1): *x*-polarized at λ = 850 nm (*y*-polarized at λ = 1550 nm) waves are reflected into + 1 (0) diffraction order. (b, c) Theoretical performance of the metasurface for *x*-polarization, displaying b) the *x*-component of the reflected E-field (E_{rx}) at the designed wavelength of 850 nm (the amplitude of the incident E-field is 1 V/m), and c) amount of incident light reflected into the different diffraction orders as a function of wavelength. (d, e) Theoretical performance of the metasurface for *y*-polarization, displaying d) the *y*-component of the reflected E-field (E_{ry}) at the designed wavelength of 1550 nm (the amplitude of the incident E-field is 1 V/m), and e) amount of incident light reflected into the different diffraction orders as a function of wavelength.

Similarly, we now design gradient metasurface (design 2) that reflects normally incident *x*-polarized at λ = 850 nm and *y*-polarized at λ = 1550 nm waves into 0 and + 1 diffraction orders, respectively. In this design, the four meta-atoms selected possess almost equal reflection phases for *x*-polarization at λ = 850 nm. Nevertheless, when the incident light is *y*-polarized, meta-atoms have different reflection phases with a step of 90°, forming a phase gradient along the *x*-direction when the wavelength is equal to 1550 nm. Consequently, the corresponding gradient metasurface can be constructed by placing the four elements into a supercell with a periodicity of 2000 nm [Fig. 3(a)], where the chosen elements are arranged in pairs in order to guide the reflected into the propagating wave rather than surface wave [14]. Numerical simulations of the designed gradient metasurface show that practically the majority of the reflected light for *y*-polarization is routed to the + 1 diffraction order with an angle of 50.8° at the designed wavelength of λ = 1550 nm [Figs. 3(d) and 3(e)]. Here it should be noted that the distortion of the reflected wave-front for *y*-polarization is ascribed to the

Optics EXPRESS

increased variations in reflection amplitude producing by the different elements comprising the supercell, which affect the performance a little bit. On the contrary, nearly all the incident light is normally reflected for x-polarization at λ = 850 nm, with the total reflectivity being limited to ~88% [Figs. 3(b) and 3(c)].

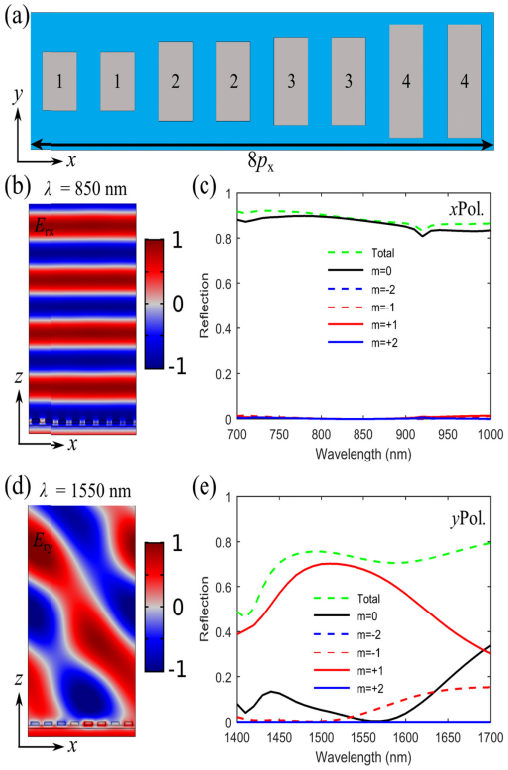

Fig. 3. (a) Supercell the polarization-sensitive dual-wavelength GSPM functioning as a polarization beam splitter (design 2): x-polarized at λ = 850 nm (y-polarized at λ = 1550 nm) waves are reflected into 0 (+ 1) diffraction order. (b, c) Theoretical performance of the metasurface for x-polarization, displaying b) the x-component of the reflected E-field (E_{rx}) at the designed wavelength of 850 nm (the amplitude of the incident E-field is 1 V/m), and c) amount of incident light reflected into the different diffraction orders as a function of wavelength. (d, e) Theoretical performance of the metasurface for y-polarization, displaying d) the y-component of the reflected E-field (E_{ry}) at the designed wavelength of 1550 nm (the amplitude of the incident E-field is 1 V/m), and e) amount of incident light reflected into the different diffraction orders as a function of wavelength.

In practical application, beam splitter that can anomalously reflected x-polarized and y-polarized waves to different directions is preferred. According to the generalized laws of reflection and refraction [6], the angle of anomalous reflection is determined by the corresponding phase gradient. As such, we can construct a polarization and wavelength beam splitter by designing a gradient metasurface with linear phase gradients that are different for the two incident polarizations. For the sake of simplicity, we still discretize the reflection phase for x- and y-polarizations into four contour lines with a 90° step and place eight meta-atoms in a supercell, shown in Fig. 4(a). The supercell composed of eight elements provides a 4π phase span with a constant phase shift of 90° for x-polarized incident light at λ = 850 nm, resulting in effective diffraction into + 2 order with an angle of 58.2° [Fig. 4(b)]. Note that the more meta-atoms introduced means more variations in the reflection amplitude, which may, in turn, decrease the performance slightly, for instance, introducing a more apparent stair-casing of the linear-phase profile. At the same time, the supercell supplies only 2π phase coverage, which is achieved by maintaining a similar y-dimension for the two neighboring

Optics EXPRESS

elements that thereby possess the equal reflection phases. Therefore, under *y*-polarized illumination at a wavelength of 1550 nm, the normally incident light will be anomalously reflected at an angle of −50.8°, which corresponds to the −1 diffraction order regarding the supercell with a periodicity of 2000 nm [Fig. 4(d)]. From Figs. 4(b) and 4(d) one can clearly see how the two orthogonal polarizations at two discrete wavelengths are reflected at the opposite sides of the surface normal with different angles, corresponding to the + 2 and −1 orders, respectively. To further analyze the performance, the amount of the reflected light into different orders is calculated as a function of wavelength [Figs. 4(c) and 4(e)]. In accord with the hypothesis, almost all reflected light goes to + 2 diffraction order for *x*-polarization at the designed wavelength of 850 nm. Importantly, it is clear that the gradient metasurface shows a broadband response with reasonable performance in the wavelength range of 750-950 nm, where most of the reflected light is routed to the + 2 diffraction and other diffraction orders are greatly suppressed. For *y*-polarization at λ = 1550 nm, the performance is slightly decreased with ~90% of the reflected light being directed to the −1 diffraction order. Similarly, we see a slight narrower operation bandwidth from 1500 to 1600 nm, which is ascribed to the degradation of the meta-atoms in the long-wavelength range.

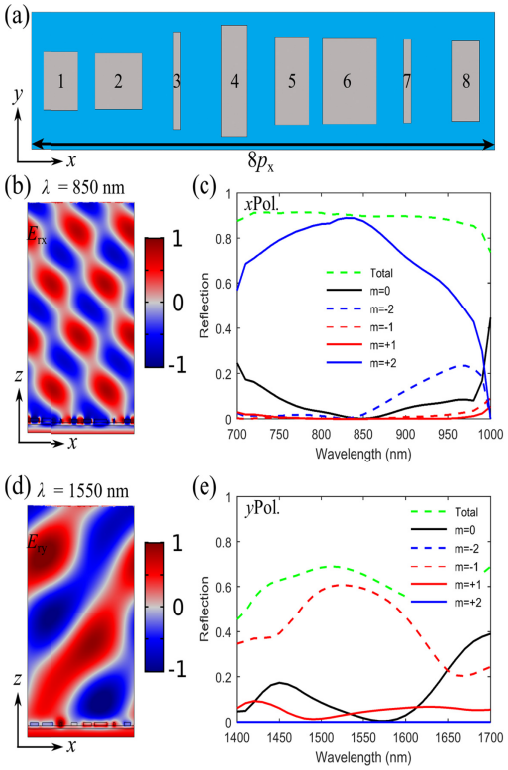

Fig. 4. (a) Supercell of the polarization-sensitive dual-wavelength GSPM functioning as a polarization beam splitter (design 3): *x*-polarized at λ = 850 nm (*y*-polarized at λ = 1550 nm) waves are reflected into + 2 (−1) diffraction order. (b, c) Theoretical performance of the metasurface for *x*-polarization, displaying b) the *x*-component of the reflected E-field (E_{rx}) at the designed wavelength of 850 nm (the amplitude of the incident E-field is 1 V/m), and c) amount of incident light reflected into the different diffraction orders as a function of wavelength. (d, e) Theoretical performance of the metasurface for *y*-polarization, displaying d) the *y*-component of the reflected E-field (E_{ry}) at the designed wavelength of 1550 nm (the amplitude of the incident E-field is 1 V/m), and e) amount of incident light reflected into the different diffraction orders as a function of wavelength.

Optics EXPRESS

4. Polarization-selective dual-band focusing metamirror

In addition to the aforementioned polarization beam splitter, the proposed polarization-sensitive dual-wavelength GSPM can be applied in more complicated wavefront shaping. As a proof-of-concept demonstration, we have designed a one-dimensional (1D) focusing metamirror working at λ = 850 and 1550 nm simultaneously. The flat mirror is a widely used optical component in energy harvesting and imaging applications, which can focus normally incident light axis at certain points. The flat 1D metamirror that focus the incident light in the *x*-*z* plane should follow the hyperbolic phase profile given by

$$\varphi(x) = \frac{2\pi}{\lambda_0}(\sqrt{x^2 + f^2} - f) \tag{1}$$

where λ_0 is the wavelength in free space and f is the focal length of the focusing metamirror. Following the hyperbolic phase distribution, the metamirror is designed with a lateral dimension of 9 μm and the same focal length f = 5 μm for both working wavelengths, corresponding to a numerical aperture (NA) of ~0.67. Specifically, the metamirror consists of 37 meta-atoms along the *x*-direction, whose dimensions are selected from the constant-phase line intersections in Fig. 1(c). The overall performance of the metamirror was evaluated by full-wave simulations, where the structure is infinitely extended in the *y*-direction. In the simulation, the *x*-polarized (*y*-polarized) Gaussian input beam was taken to be invariant along the *y*-direction and PMLs were used in the *x*- and *z*-directions. From Fig. 5, one can clearly see the strong focusing effect at the designed focal length for both 850 and 1550 nm, where the diffraction-limited spots are formed. At the long wavelength of λ = 1550 nm, the focal spot becomes larger with lower intensity. Furthermore, similar to the polarization beam splitters, the designed focusing metamirror exhibits the broadband response featuring good focusing characteristics.

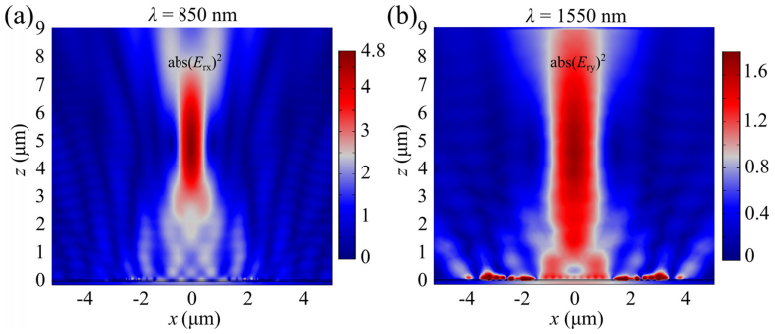

Fig. 5. Simulated intensity distribution of the reflected light, which shows the performance of the 1D dual-band focusing metamirror at the working wavelengths of a) 850 nm and b) 1550 nm based on dual-wavelength GSPM under Gaussian wave illumination at normal incidence for different polarizations. The amplitude of the incident E-field is 1 V/m and the color bar is normalized to the incident intensity.

5. Conclusions

In conclusion, we have proposed a general method to realize optical GSPMs composed of periodic anisotropic meta-atoms arranged in a rectangular lattice, which have two degrees of freedom to independently control the reflection phase and amplitude of orthogonal linear polarizations at two discrete wavelengths. We have designed and demonstrated polarization beam splitters and focusing metamirror operating at 850 and 1550 nm simultaneously, depending on the incident polarizations. Our work provides a general approach to design multi-wavelength, multifunctional metasurfaces with various potential applications.

Optics EXPRESS

Funding

National Natural Science Foundation of China (Grant Nos.11604167, 61501499) and K. C. Wong Magna Fund in Ningbo University, Foundation of Navigation Grant 20151896014.

References

1. A. V. Kildishev, A. Boltasseva, and V. M. Shalaev, "Planar photonics with metasurfaces," Science **339**(6125), 1232009 (2013).
2. N. Yu and F. Capasso, "Flat optics with designer metasurfaces," Nat. Mater. **13**(2), 139–150 (2014).
3. S. B. Glybovski, S. A. Tretyakov, P. A. Belov, Y. S. Kivshar, and C. R. Simovski, "Metasurface: from microwave to visible," Phys. Rep. **634**, 1–72 (2016).
4. H.-T. Chen, A. J. Taylor, and N. Yu, "A review of metasurfaces: physics and applications," Rep. Prog. Phys. **79**(7), 076401 (2016).
5. F. Ding, A. Pors, and S. I. Bozhevolnyi, "Gradient metasurfaces: a review of fundamentals and applications," Rep. Prog. Phys. **81**(2), 026401 (2018).
6. N. Yu, P. Genevet, M. A. Kats, F. Aieta, J.-P. Tetienne, F. Capasso, and Z. Gaburro, "Light propagation with phase discontinuities: Generalized laws of reflection and refraction," Science **334**(6054), 333–337 (2011).
7. X. Ni, N. K. Emani, A. V. Kildishev, A. Boltasseva, and V. M. Shalaev, "Broadband light bending with plasmonic nanoantennas," Science **335**(6067), 427 (2012).
8. S. Sun, K. Y. Yang, C. M. Wang, T. K. Juan, W. T. Chen, C. Y. Liao, Q. He, S. Xiao, W. T. Kung, G. Y. Guo, L. Zhou, and D. P. Tsai, "High-efficiency broadband anomalous reflection by gradient meta-surfaces," Nano Lett. **12**(12), 6223–6229 (2012).
9. C. Pfeiffer and A. Grbic, "Metamaterial Huygens' surfaces: Tailoring wave fronts with reflectionless sheets," Phys. Rev. Lett. **110**(19), 197401 (2013).
10. A. Pors, O. Albrektsen, I. P. Radko, and S. I. Bozhevolnyi, "Gap plasmon-based metasurfaces for total control of reflected light," Sci. Rep. **3**(1), 2155 (2013).
11. T. J. Cui, M. Q. Qi, X. Wan, J. Zhao, and Q. Cheng, "Coding metamaterials, digital metamaterials and programmable metamaterials," Light Sci. Appl. **3**(10), e218 (2014).
12. W. Luo, S. Xiao, Q. He, S. Sun, and L. Zhou, "Photonic Spin Hall Effect with Nearly 100% Efficiency," Adv. Opt. Mater. **3**(8), 1102–1108 (2015).
13. A. Pors, F. Ding, Y. Chen, I. P. Radko, and S. I. Bozhevolnyi, "Random-phase metasurfaces at optical wavelengths," Sci. Rep. **6**(1), 28448 (2016).
14. S. Sun, Q. He, S. Xiao, Q. Xu, X. Li, and L. Zhou, "Gradient-index meta-surfaces as a bridge linking propagating waves and surface waves," Nat. Mater. **11**(5), 426–431 (2012).
15. L. Huang, X. Chen, B. Bai, Q. Tan, G. Jin, T. Zentgraf, and S. Zhang, "Helicity dependent directional surface plasmon polariton excitation using a metasurface with interfacial phase discontinuity," Light Sci. Appl. **2**(3), e70 (2013).
16. A. Pors, M. G. Nielsen, T. Bernardin, J. C. Weeber, and S. I. Bozhevolnyi, "Efficient unidirectional polarization-controlled excitation of surface plasmon polaritons," Light Sci. Appl. **3**(8), e197 (2014).
17. W. Sun, Q. He, S. Sun, and L. Zhou, "High-efficiency surface plasmon meta-couplers: concept and microwave-regime realizations," Light Sci. Appl. **5**(1), e16003 (2016).
18. W. T. Chen, K. Y. Yang, C. M. Wang, Y. W. Huang, G. Sun, I. D. Chiang, C. Y. Liao, W. L. Hsu, H. T. Lin, S. Sun, L. Zhou, A. Q. Liu, and D. P. Tsai, "High-efficiency broadband meta-hologram with polarization-controlled dual images," Nano Lett. **14**(1), 225–230 (2014).
19. G. Zheng, H. Mühlenbernd, M. Kenney, G. Li, T. Zentgraf, and S. Zhang, "Metasurface holograms reaching 80% efficiency," Nat. Nanotechnol. **10**(4), 308–312 (2015).
20. X. Li, L. Chen, Y. Li, X. Zhang, M. Pu, Z. Zhao, X. Ma, Y. Wang, M. Hong, and X. Luo, "Multicolor 3D meta-holography by broadband plasmonic modulation," Sci. Adv. **2**(11), e1601102 (2016).
21. S. Choudhury, U. Guler, A. Shaltout, V. M. Shalaev, A. V. Kildishev, and A. Boltasseva, "Pancharatnam-Berry phase manipulating metasurface for visible color hologram based on low loss silver thin film," Adv. Opt. Mater. **5**(10), 1700196 (2017).
22. X. Chen, L. Huang, H. Mühlenbernd, G. Li, B. Bai, Q. Tan, G. Jin, C. W. Qiu, S. Zhang, and T. Zentgraf, "Dual-polarity plasmonic metalens for visible light," Nat. Commun. **3**(1), 1198 (2012).
23. A. Pors, M. G. Nielsen, R. L. Eriksen, and S. I. Bozhevolnyi, "Broadband focusing flat mirrors based on plasmonic gradient metasurfaces," Nano Lett. **13**(2), 829–834 (2013).
24. M. D. Huntington, L. J. Lauhon, and T. W. Odom, "Subwavelength lattice optics by evolutionary design," Nano Lett. **14**(12), 7195–7200 (2014).
25. M. Khorasaninejad, W. T. Chen, R. C. Devlin, J. Oh, A. Y. Zhu, and F. Capasso, "Metalenses at visible wavelengths: Diffraction-limited focusing and subwavelength resolution imaging," Science **352**(6290), 1190–1194 (2016).
26. A. Pors, M. G. Nielsen, and S. I. Bozhevolnyi, "Broadband plasmonic half-wave plates in reflection," Opt. Lett. **38**(4), 513–515 (2013).

Optics EXPRESS

27. N. K. Grady, J. E. Heyes, D. R. Chowdhury, Y. Zeng, M. T. Reiten, A. K. Azad, A. J. Taylor, D. A. R. Dalvit, and H. T. Chen, "Terahertz metamaterials for linear polarization conversion and anomalous refraction," Science **340**(6138), 1304–1307 (2013).
28. F. Ding, Z. Wang, S. He, V. M. Shalaev, and A. V. Kildishev, "Broadband high-efficiency half-wave plate: A supercell-based plasmonic metasurface approach," ACS Nano **9**(4), 4111–4119 (2015).
29. A. Pors, M. G. Nielsen, and S. I. Bozhevolnyi, "Plasmonic metagratings for simultaneous determination of stokes parameters," Optica **2**(8), 716–723 (2015).
30. E. Maguid, I. Yulevich, D. Veksler, V. Kleiner, M. L. Brongersma, and E. Hasman, "Photonic spin-controlled multifunctional shared-aperture antenna array," Science **352**(6290), 1202–1206 (2016).
31. F. Ding, A. Pors, Y. Chen, V. A. Zenin, and S. I. Bozhevolnyi, "Beam-size-invariant spectropolarimeters using gap-plasmon metasurfaces," ACS Photonics **4**(4), 943–949 (2017).
32. F. Ding, Y. Chen, and S. I. Bozhevolnyi, "Metasurface-based polarimeters," Appl. Sci. **8**(4), 594 (2018).
33. C. Zhang, F. Yue, D. Wen, M. Chen, Z. Zhang, W. Wang, and X. Chen, "Multichannel metasurface for simultaneous control of holograms and twisted light beams," ACS Photonics **4**(8), 1906–1912 (2017).
34. S. Tang, T. Cai, H. Xu, Q. He, S. Sun, and L. Zhou, "Multifunctional metasurfaces based on the "merging" concept and anisotropic single-structure meta-atoms," Appl. Sci. **8**(4), 555 (2018).
35. M. Q. Mehmood, S. Mei, S. Hussain, K. Huang, S. Y. Siew, L. Zhang, T. Zhang, X. Ling, H. Liu, J. Teng, A. Danner, S. Zhang, and C. W. Qiu, "Visible-frequency metasurface for structuring and spatially multiplexing optical vortices," Adv. Mater. **28**(13), 2533–2539 (2016).
36. S. Zhong, L. Wu, T. Liu, J. Huang, W. Jiang, and Y. Ma, "Transparent transmission-selective radar-infrared bi-stealth structure," Opt. Express **26**(13), 16466–16476 (2018).
37. B. Desiatov, N. Mazurski, Y. Fainman, and U. Levy, "Polarization selective beam shaping using nanoscale dielectric metasurfaces," Opt. Express **23**(17), 22611–22618 (2015).
38. H. X. Xu, S. Tang, G. M. Wang, T. Cai, W. Huang, Q. He, S. Sun, and L. Zhou, "Multifunctional microstrip array combining a linear polarizer and focusing metasurface," IEEE Trans. Antenn. Propag. **64**(8), 3676–3682 (2016).
39. T. Cai, S. W. Tang, G. M. Wang, H. X. Xu, S. L. Sun, Q. He, and L. Zhou, "High-performance bifunctional metasurfaces in transmission and reflection geometries," Adv. Opt. Mater. **5**(2), 1600506 (2017).
40. T. Cai, G. M. Wang, S. W. Tang, H. X. Xu, J. W. Duan, H. J. Guo, F. X. Guan, S. L. Sun, Q. He, and L. Zhou, "High-efficiency and full-space manipulation of electromagnetic wave fronts with metasurfaces," Phys. Rev. Appl. **8**(3), 034033 (2017).
41. H. X. Xu, S. Tang, X. Ling, W. Luo, and L. Zhou, "Flexible control of highly-directive emissions based on bifunctional metasurfaces with low polarization cross-talking," Ann. Phys-Berlin **529**(5), 1700045 (2017).
42. T. Cai, G. M. Wang, H. X. Xu, S. W. Tang, and J. G. Liang, "Polarization-independent broadband meta-surface for bifunctional antenna," Opt. Express **24**(20), 22606–22615 (2016).
43. F. Ding, R. Deshpande, and S. I. Bozhevolnyi, "Bifunctional gap-plasmon metasurfaces for visible light: polarization-controlled unidirectional surface plasmon excitation and beam steering at normal incidence," Light Sci. Appl. **7**(4), 17178 (2018).
44. Y. W. Huang, W. T. Chen, W. Y. Tsai, P. C. Wu, C. M. Wang, G. Sun, and D. P. Tsai, "Aluminum plasmonic multicolor meta-hologram," Nano Lett. **15**(5), 3122–3127 (2015).
45. E. Arbabi, A. Arbabi, S. M. Kamali, Y. Horie, and A. Faraon, "Multiwavelength polarization-insensitive lenses based on dielectric metasurfaces with meta-molecules," Optica **3**(6), 628–633 (2016).
46. F. Aieta, M. A. Kats, P. Genevet, and F. Capasso, "Multiwavelength achromatic metasurfaces by dispersive phase compensation," Science **347**(6228), 1342–1345 (2015).
47. B. Wang, F. Dong, Q. T. Li, D. Yang, C. Sun, J. Chen, Z. Song, L. Xu, W. Chu, Y. F. Xiao, Q. Gong, and Y. Li, "Visible-frequency dielectric metasurfaces for multiwavelength achromatic and highly dispersive holograms," Nano Lett. **16**(8), 5235–5240 (2016).
48. B. H. Chen, P. C. Wu, V. C. Su, Y. C. Lai, C. H. Chu, I. C. Lee, J. W. Chen, Y. H. Chen, Y. C. Lan, C. H. Kuan, and D. P. Tsai, "GaN metalens for pixel-level full-color routing at visible light," Nano Lett. **17**(10), 6345–6352 (2017).
49. W. Ma, Z. Huang, X. K. Bai, P. Zhan, and Y. M. Liu, "Dual-band light focusing using stacked graphene metasurfaces," ACS Photonics **4**(7), 1770–1775 (2017).
50. J. Ding, S. An, B. Zheng, and H. Zhang, "Multiwavelength metasurfaces based on single-layer dual-wavelength meta-atoms: toward complete phase and amplitude modulations at two wavelengths," Adv. Opt. Mater. **5**(10), 1700079 (2017).
51. J. Yang, C. Huang, X. Wu, B. Sun, and X. Luo, "Dual-wavelength carpet cloak using ultrathin metasurface," Adv. Opt. Mater. **6**(14), 1800073 (2018).
52. O. Eisenbach, O. Avayu, R. Ditcovski, and T. Ellenbogen, "Metasurfaces based dual wavelength diffractive lenses," Opt. Express **23**(4), 3928–3936 (2015).
53. E. Arbabi, A. Arbabi, S. M. Kamali, Y. Horie, and A. Faraon, "High efficiency double-wavelength dielectric metasurface lenses with dichroic birefringent meta-atoms," Opt. Express **24**(16), 18468–18477 (2016).
54. J. B. Pendry, A. J. Holden, D. J. Robbins, and W. J. Stewart, "Magnetism from conductors and enhanced non-linear phenomena," IEEE Trans. Microw. Theory Tech. **47**(11), 2075–2084 (1999).
55. J. M. Hao, L. Zhou, and C. T. Chan, "An effective-medium model for high-impedance surfaces," Appl. Phys., A Mater. Sci. Process. **87**(2), 281–284 (2007).

Optics EXPRESS

56. J. Hao, J. Wang, X. Liu, W. J. Padilla, L. Zhou, and M. Qiu, "High performance optical absorber based on a plasmonic matematerial," Appl. Phys. Lett. **96**(25), 251104 (2010).
57. N. Liu, M. Mesch, T. Weiss, M. Hentschel, and H. Giessen, "Infrared perfect absorber and its application as plasmonic sensor," Nano Lett. **10**(7), 2342–2348 (2010).
58. A. Pors and S. I. Bozhevolnyi, "Plasmonic metasurfaces for efficient phase control in reflection," Opt. Express **21**(22), 27438–27451 (2013).
59. F. Ding, Y. Yang, R. Deshpande, and S. I. Bozhevolnyi, "A review of gap-surface plasmon metasurfaces: fundamentals and applications," Nanophotonics **7**(6), 1129–1156 (2018).
60. X. Pan, H. Xu, Y. Gao, Y. Zhang, L. Sun, D. Li, Z. Wen, S. Li, W. Yu, Z. Huang, J. Wang, B. Zhang, Y. Sun, J. Sun, X. Meng, X. Chen, B. Dagens, J. Hao, Y. Shen, N. Dai, and J. Chu, "Spatial and frequency selective plasmonic metasurface for long wavelength infrared spectral region," Adv. Opt. Mater. 1800337 (2018).